J. exp. Biol. 108, 205–230 (1984)
Printed in Great Britain © The Company of Biologists Limited 1984

MOVEMENTS AND ACTIVE MOMENTS OF BULL SPERM FLAGELLA AS A FUNCTION OF TEMPERATURE AND VISCOSITY

By ROBERT RIKMENSPOEL

Department of Biological Sciences, State University of New York, Albany, NY 12222, U.S.A.

Accepted 24 May 1983

SUMMARY

Detailed measurements were made of the movements and waveforms of bull sperm flagella over a temperature range of 5 to 37 °C and over a range of external viscosities of $1–3600 \times 10^{-3}$ Pa s^{-1}*. The data obtained were used for an evaluation of the internal active moments in the flagella, using exact, large amplitude, algebra. The results of the calculations show that the axoneme in bull sperm flagella can produce the forces necessary to power the flagellar motion over the entire range of conditions. The calculations further suggest that no other structure in the bull sperm flagella has a force-producing function.

INTRODUCTION

In the flagella of mammalian sperm, the central axoneme is surrounded by a set of nine auxilliary fibres, often called coarse fibres. In many species such as bull and guinea pig, these fibres have a large diameter of approximately 100 nm in the proximal part of the flagellum, and taper gradually towards the distal tip (Friend, Elias & Rudolf, 1979; Fawcett, 1975; Phillips, 1972).

It is now generally assumed that the coarse fibres contribute an extra structural rigidity to mammalian flagella above that provided by the central axoneme (Phillips, 1972; Lindemann, Rudd & Rikmenspoel, 1973; Baccetti, Pallini & Burrini, 1976). It has not been unequivocally settled, however, whether the coarse fibres also contribute to force production during the motility of the flagella.

Reports on the presence of ATPase activity in the auxiliary fibres have appeared from time to time (Engelhardt & Burnasheva, 1957; Burnasheva, 1958; Nelson, 1962; Baccetti, Pallini & Burrini, 1973). The techniques employed in these experiments were usually histochemical, and they could not, therefore, quantitatively establish the amount of ATPase activity. Direct measurements in preparations of more or less purified coarse fibres have failed to demonstrate the presence of an ATPase (Price, 1973; Pihlaja & Roth, 1973; Baccetti *et al.* 1976). As pointed out by Baccetti *et al.* (1973) it is not excluded, however, that the extraction procedures used had destroyed the ATPase activity.

* For conversion to conventional units: 10^{-3} Pa s^{-1} = 1 cpoise; 10^{-5} N = 1 dyne; 10^{-7} J = 1 erg.

Key words: Bull sperm flagella, active moments, coarse fibres.

The internal, active, moments produced in the flagella of both invertebrate and mammalian sperm have been calculated by several investigators. The values obtained for the active moments in invertebrate sperm flagella, which consist essentially only of the axonemal dynein-tubulin system (Summers & Gibbons, 1971), were typically of the order of $1–1{\cdot}5 \times 10^{-14}$ N cm (Hiramoto & Baba, 1978; Rikmenspoel, 1978*a*, 1982). For bull spermatozoa, this author has reported internal active moments ranging from $3–6 \times 10^{-14}$ N cm (Rikmenspoel, Jacklet, Orris & Lindemann, 1973; Rikmenspoel, 1978*a*). These latter values were obtained with analyses in small amplitude approximation. Furthermore, the data, from the observed motion of bull sperm flagella, on which the calculations were based, were not of a high quality. It was thus stated (Rikmenspoel, 1978*a*) that the absolute values of the active moments in bull sperm should be treated with caution.

The rate of the energy metabolism in bull spermatozoa has been measured as approximately 30×10^{-18} mol ATP s^{-1} $sperm^{-1}$ (Rikmenspoel, Sinton & Janick, 1969; Nevo & Rikmenspoel, 1970). For the invertebrate *Ciona* sperm, Brokaw & Benedict (1968) have reported an ATP turnover of approximately 6×10^{-18} mol ATP s^{-1} $sperm^{-1}$. In the case of bull sperm, the rate of ATP hydrolysis was normalized to the number of moving sperm in the samples; for the *Ciona* sperm it referred to the total number of sperm. Since semen samples always contain a sizeable fraction of immotile (and presumable dead) sperm, the ATP turnover per moving *Ciona* sperm could be of the order of 10×10^{-18} mol ATP s^{-1} $sperm^{-1}$. The value for the ATP turnover rate in bull sperm was measured at 37 °C, that for *Ciona* sperm at 16 °C. As emphasized by Lindemann & Gibbons (1975), the apparently higher ATPase activity in bull sperm can, therefore, not be taken as evidence for a higher content of ATPase molecules without an investigation of the effects of temperature on the metabolic rates.

The evidence summarized above, while pointing to the possibility of an extra-axonemal force-producing mechanism in mammalian sperm, should be considered inconclusive. Experiments designed to contribute to resolving this question are described in this paper. Accurate observations were made of the motion of bull spermatozoa over a wide range of temperature and viscosity. The data were used as the basis for calculations of the active moments in the sperm flagella employing exact, large amplitude algebra. The results show clearly that the axonemal dynein-tubulin system is capable of producing the active moments necessary to maintain the motility. They further suggest that no other structures in the bull sperm flagellum contribute to the internal active moments.

METHODS

Sperm preparations and media

Bull spermatozoa were generously provided by the Eastern Artificial Insemination Cooperative at Ithaca, NY. After collection, the semen was diluted five times with an optically clear egg yolk citrate diluent described previously (Rikmenspoel, 1957), cooled to 4 °C and transported to the laboratory. Immediately prior to the experiments, the sperm were washed once by centrifuging at 800 ***g*** for 2 min and resuspending the pellet in a basic medium (BM) containing 72 mM-KCl, 160 mM-sucrose

2 mM-Na-pyruvate and 2% of 0·1 M-Na-phosphate buffer, at pH 7·4 (O'Day & Rikmenspoel, 1979).

For motility measurements at varying temperatures, several drops of the washed semen were stirred into 2 ml of BM. For the experiments at high viscosity, 8 drops of washed semen were mixed into 1 ml of BM, and 0·2 ml of this mixture was slowly stirred with a magnetic stirrer into 2 ml of the high viscosity medium described below.

Raised viscosity

High viscosity media (up to 4 Pa s^{-1}) were prepared by mixing up to 2% of high viscosity carboxymethyl cellulose (Sigma Chemical Company, St. Louis, Missouri) into the BM. The viscosity of each high viscosity semen sample was measured with a falling ball microviscometer described before (Lindemann & Rikmenspoel, 1972). Since the shearing rates in the fluid surrounding a moving sperm flagellum were similar to those in our viscometer, no corrections for shearing rate (Pate & Brokaw, 1980) were judged necessary.

Microscopy and cinemicrography

Microscopic samples were prepared by placing 4 drops of the washed, diluted semen on acid washed slides. After placement of a cover glass the resulting fluid layer was at least 30 μm thick. This ensured unhindered motion of the sperm flagella.

The preparations were viewed in darkfield with a Zeiss 40× water immersion objective, as described before (Nichols & Rikmenspoel, 1977). At the sperm concentration used, from one to five sperm were visible in the field of view.

The temperature of the samples was controlled by a water-circulated stage, covered by a Lucite enclosure (Rikmenspoel *et al.* 1969). The temperature of the slides was measured with a thermistor microprobe (Yellow Springs Instrument Co., Yellow Springs, Ohio).

Cinemicrographs at 200–20 frames s^{-1} were made on Kodak Plus X emulsion at a final magnification of approximately 50× as described previously (Nichols & Rikmenspoel, 1977). The framing rate was chosen for each experiment such that at least 10 frames were taken during each period of the flagellar motion.

Data analysis

Bull spermatozoa display either a helical, three-dimensional flagellar wave accompanied by a steady rotation of the whole sperm on its longitudinal axis, or a planar, two-dimensional wave. In this latter case the sperm swim along a circular path (Rikmenspoel, Van Herpen & Eykhout, 1960; Rikmenspoel, 1965). It has been found previously in this laboratory that a quantitative analysis of the flagellar wave in the rotating sperm leads to considerable difficulties in interpretation and results in rather sizeable inaccuracies of the data (Rikmenspoel, 1965; Rikmenspoel *et al.* 1973). For this reason, only sperm with a flat flagellar wave were analysed in the present experiments.

Films were projected to a final magnification of 2000×. The films were scanned and the flagellar frequency was measured for all sperm with a planar flagellar wave. For each experimental condition, from five to eight cells were selected for detailed analysis. The sperm were chosen such that the average frequency in each group was

close to the average flagellar frequency of all sperm for the particular experimental condition.

The flagellar images of the selected sperm were traced on paper for two to three consecutive periods of motion. The average path of each sperm was determined as the centre line of superimposed tracings. Small dust spots and imperfections on the slides were used as fiducial markers. As illustrated in Fig. 1, segments of 5 μm long were marked off on the flagellar images. The deviations from the average path at 0, 10, 20, 30, 40 and 50 μm from the head-flagellar junction were plotted as a function of time. For each of the locations on the flagellum, a wavy curve of the transverse motion (the amplitude) *versus* time was thus obtained, as shown in Fig. 2A for a

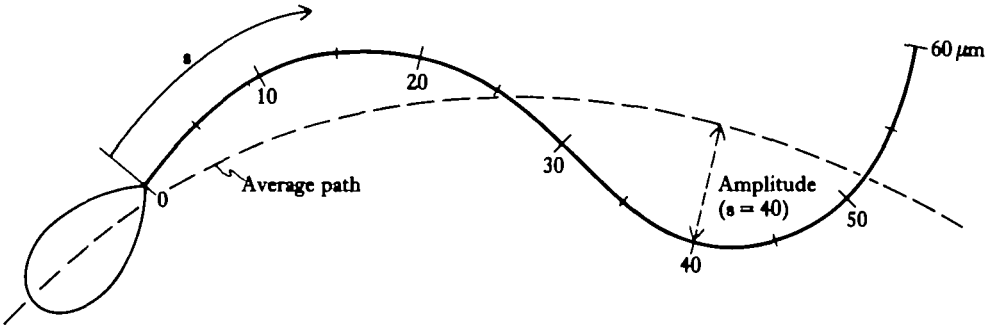

Fig. 1. Tracing of a bull sperm illustrating the measurement of the transverse deviation from the average path of the sperm (the amplitude), as a function of the curvilinear distance, s, from the head of the sperm.

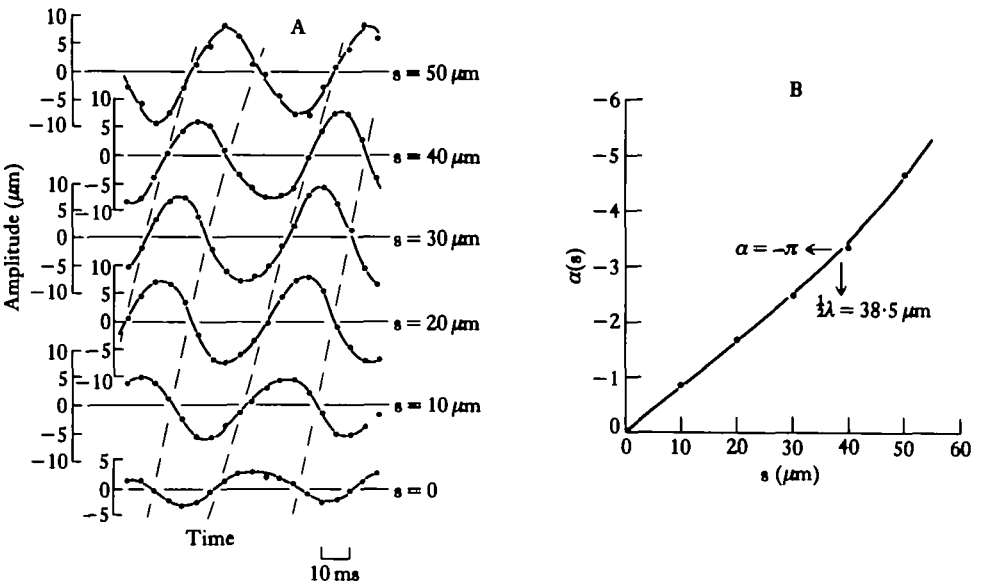

Fig. 2. (A) Amplitude at various locations on the flagellum of a bull sperm at 37 °C as a function of time. The dashed lines connect the crossover points of the amplitude curves and show the progression of the flagellar wave. (B) Progression of the flagellar wave of the sperm in (A) expressed as the average phase, $\alpha(s)$, of the crossover points of the amplitude curves in (A). The value of s where $\alpha(s) = -\pi$ gives the length of the first half wave on the flagellum.

sperm at 37 °C in normal viscosity. Fig. 2A illustrates the quality of the data obtained.

Each of the curves in Fig. 2A can be represented roughly by a sine curve: $U = A(s) \sin \omega t$, where U, the amplitude, is the deviation from the average path, A(s) is the maximum amplitude at location s, ω is the angular frequency of the sperm and t is the time. The progression of the wave along the flagellum can be seen by the increasing phase shift with s of the curves in Fig. 2A. If the phase shift for each curve in Fig. 2A is written as $\alpha(s)$, normalized to $\alpha(0) = 0$, all curves in Fig. 2A may be summarized as

$$U(s,t) = A(s) \sin [\omega t + \alpha(s)]. \quad (1)$$

This is analogous to the notation used previously (Rikmenspoel, 1965). However, the running coordinate s, used here and throughout this paper, is the curvilinear distance from the head measured along the flagellum.

Fig. 2B shows that the curve for $\alpha(s)$ is rather straight, except for the extreme distal part of the flagellum. This was found in all cases, except for sperm at extremely high viscosity. The value of s at which $\alpha(s) = -\pi$ yields the length of the first half wave, $\lambda/2$, measured along the flagellum. In the remainder of this paper, the wave properties will be expressed in the function A(s) of equation (1) above, and in the value of $\lambda/2$.

RESULTS

Temperature effects

Measurements were made on sperm preparations at 37, 28, 20, 11 and 5 °C. Fig. 3A shows that the flagellar frequency decreased smoothly in this range from 20·5 Hz at 37 °C to 1·1 Hz at 5 °C. An Arrhenius plot of the data (Fig. 3B) shows a straight line in the range 37–10 °C, with a Q_{10} value for the flagellar frequency of $Q_{10} = 2{\cdot}1$. Below approximately 10 °C the frequency exhibits a sudden drop in Fig. 3B. This

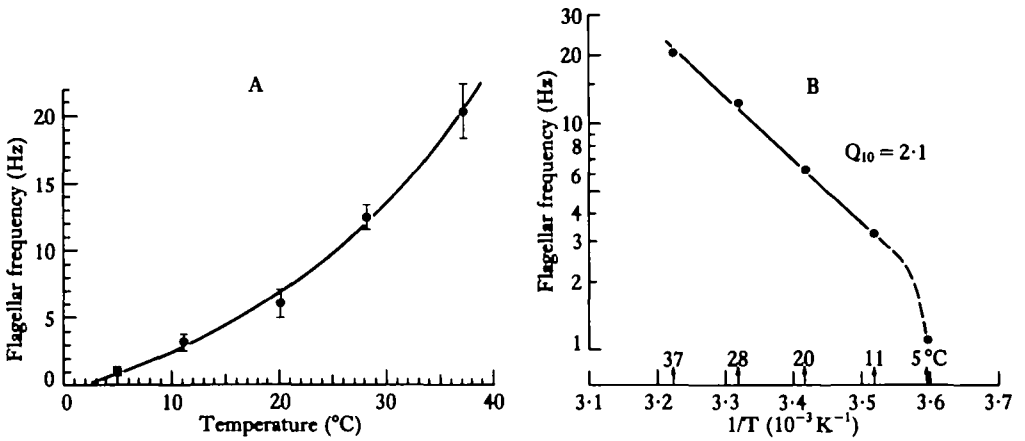

Fig. 3. (A) Flagellar frequency of bull sperm as a function of temperature. Each point represents an average over 7 to 18 sperm. The vertical bars show the standard deviation over the sperm at each temperature. (B) Arrhenius plot of the data in (A) showing a $Q_{10} = 2{\cdot}1$ for the flagellar frequency in the range 37–11 °C.

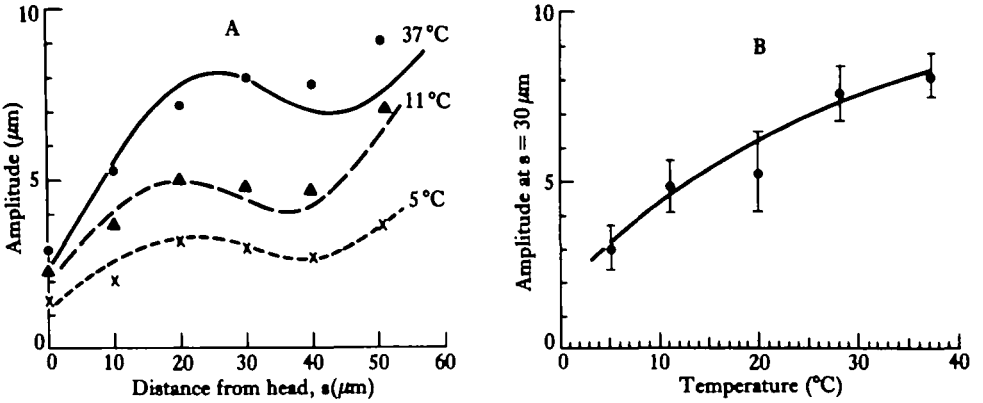

Fig. 4. (A) Amplitude as a function of the distance from the head, s, for bull sperm at 37, 11 and 5 °C. The lines are computed curves, as explained in the section *Evaluation of active moments*. (B) Amplitude at s = 30 μm of the bull sperm flagellar wave as a function of temperature. The line was drawn by eye. The vertical bars are standard deviations over the sperm at each temperature. Each point in this figure and in Fig. 5 represents an average over 5 to 8 sperm.

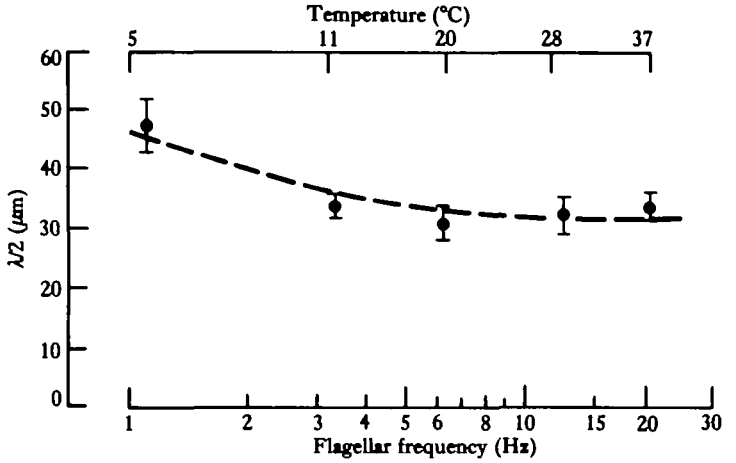

Fig. 5. Length of the first half wave, $\lambda/2$, in bull sperm flagella as a function of flagellar frequency when the changes were induced by temperature variation. The temperature corresponding to each frequency is shown at the top.

break in the Arrhenius plot for the flagellar frequency at 10 °C has been observed also by Coakley & Holwill (1974) in the organism *Crithidia oncopelti*.

At all temperatures the amplitude of the flagellar wave increased towards the distal tip, as illustrated in Fig. 4A. The amplitude at a distance s = 30 μm from the head, where the function A(s) has a plateau, is shown *versus* the temperature in Fig. 4B.

The length of the first half wave in the flagella, $\lambda/2$, varied only slowly with temperature, and therefore with the flagellar frequency, as shown in Fig. 5. This parallels the weak variation of flagellar wavelength with frequency found by Brokaw & Josslin (1973) in sea urchin sperm. In this latter case, however, the reduction in

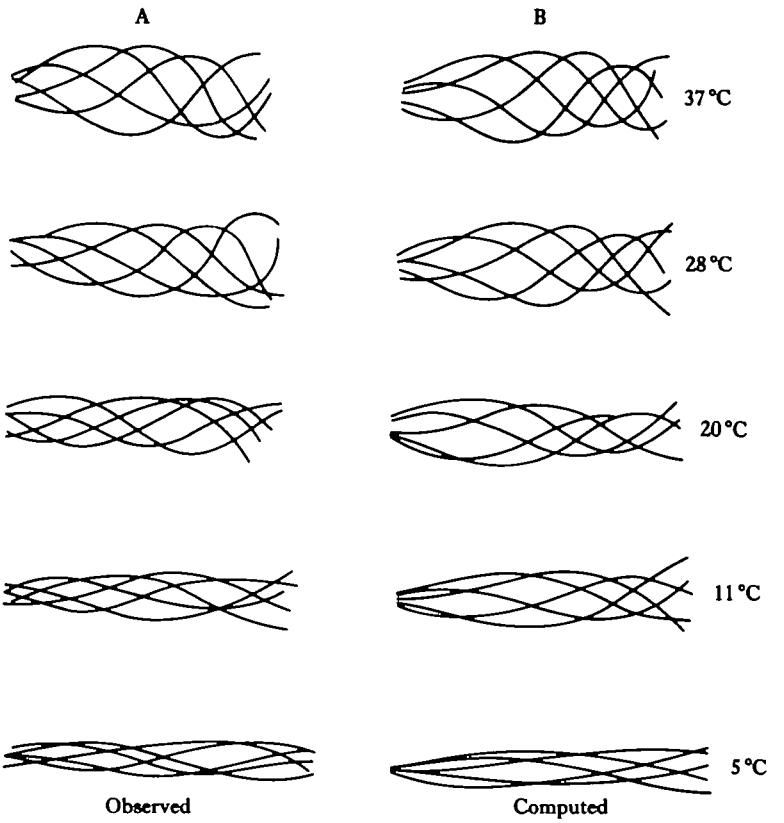

Fig. 6. (A) Typical flagellar waveforms of bull sperm at temperatures ranging from 5 to 37 °C. The forward progression of the sperm was in each case removed by shifting the tracing along the average path. The sperm were in general curved. The overall curvature was removed by cutting the tracings in strips and reassembling them in a straightened fashion, as explained previously (Rikmenspoel, 1978). (B) Waveforms at the various temperatures computed as explained in the section *Evaluation of active moments*, and with the driving force for the motion produced by the central axoneme in the flagella only. A few microns of the most proximal part of the computed waveforms were omitted.

flagellar frequency was obtained by lowering the external ATP concentration of demembranated sperm.

The combined data of Figs 3, 4 and 5 give the impression that at lowered temperatures the motile activity in bull sperm is gradually reduced, but that no essential changes in the processes in the flagella have occurred. This is supported by the appearance of the flagellar waveforms at the various temperatures shown in Fig. 6A. The sperm represented in Fig. 6A were chosen for having values of amplitude, frequency and $\lambda/2$ close to the average for the temperature.

Effects of raised viscosity

The motility of sperm was recorded at 68, 131, 330, 790 and 3600×10^{-3} Pa s^{-1}. The temperature of the preparations was maintained at 37 °C during all measurements. The data at 37 °C taken for the temperature measurements described above

were used as a control at 1×10^{-3} Pa s^{-1}. While nothing indicated that 3600×10^{-3} Pa s^{-1} was a limit above which no motility would occur, the practical difficulties of handling solutions with a viscosity much above 4000×10^{-3} Pa s^{-1} prevented experimentation at higher viscosities.

Fig. 7 shows the average flagellar frequency measured at the various viscosity values. Inserted in Fig. 7 are the flagellar frequencies reported previously (Rikmenspoel *et al.* 1973) for rotating bull sperm over a more limited viscosity range of 1 to 16×10^{-3} Pa s^{-1}. These earlier data fit well to the trend of the present results. Fig. 7 shows that over the entire viscosity range of $1–3600 \times 10^{-3}$ Pa s^{-1} the flagellar frequency, ν, in bull sperm decreases almost exactly with the square root of the viscosity, η: $\nu \propto \eta^{-1/2}$. The line drawn by eye through the data points in Fig. 7 has a slope of $-0{\cdot}48$.

The flagellar waveform changed in qualitative appearance at raised viscosity. As illustrated in Fig. 8A and B, the amplitude near the head became progressively smaller at higher viscosities, whereas the amplitude near the distal tip remained roughly constant over the entire range. This resulted in an increasingly trumpet-shaped appearance of the envelope of the flagellar wave, as shown in Fig. 10A below.

The function $\alpha(s)$, which defines the progression of the wave along the flagellum as explained with Fig. 2 above, became more curved at higher viscosities. The flagellar wave travelled more slowly than the average in the proximal part of the flagellum, and faster in the distal part. The values for the length of the first half wave in the flagellum, $\lambda/2$, shown in Fig. 9 have, therefore, only a qualitative meaning, especially at the highest viscosities, $\eta > 300 \times 10^{-3}$ Pa s^{-1}.

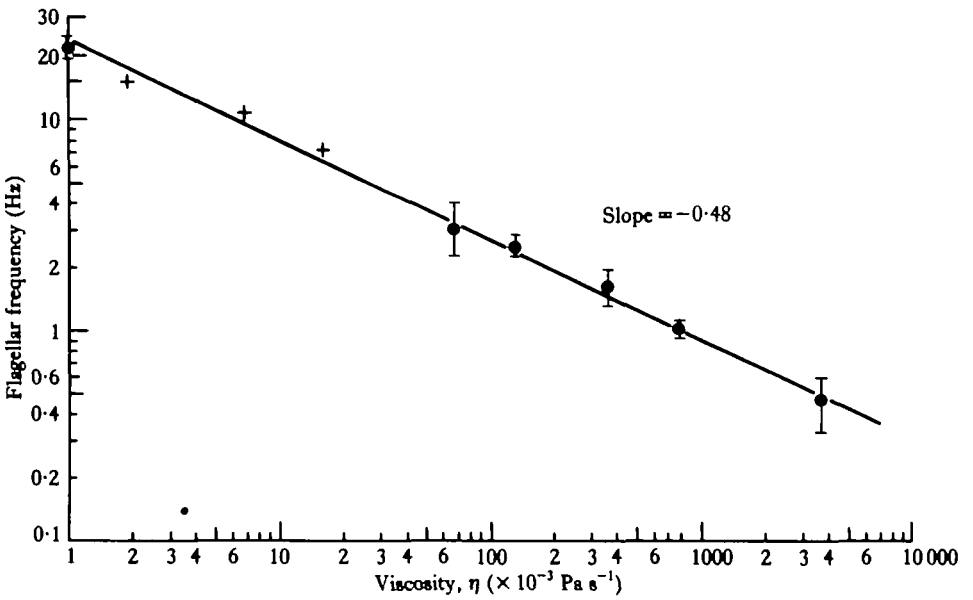

Fig. 7. Flagellar frequency of bull sperm at 37 °C as a function of the viscosity of the medium. ●, Present measurements; + data from Rikmenspoel, Jacklet, Orris & Lindemann (1973) reported previously. Each point represents the average over 8 to 12 sperm. The vertical bars are standard deviations. The line with a slope of $-0{\cdot}48$ was drawn by eye.

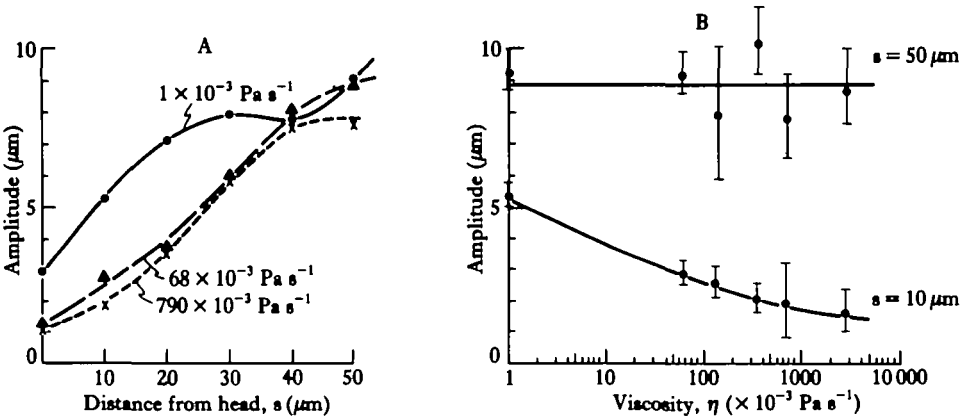

Fig. 8. (A) Flagellar amplitude of bull sperm at a viscosity of 1, 68 and 790 × 10^{-3} Pa s^{-1} as a function of the distance from the head, s. Each point in this figure and in Figs 8B and 9 represents the average over five to seven sperm. The lines in this figure and Figs 8B and 9 were drawn by eye. (B) Amplitude at s = 10 μm and s = 50 μm of bull sperm as a function of viscosity. The vertical bars are standard deviations.

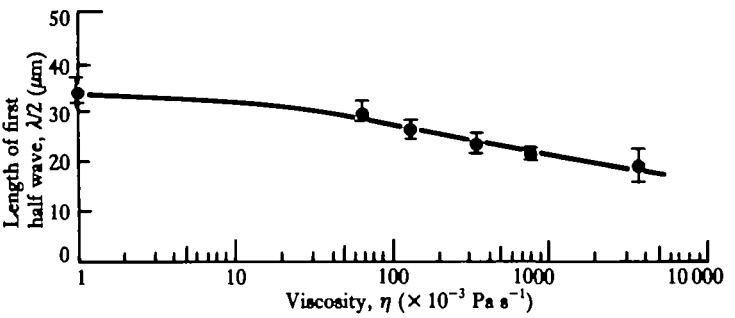

Fig. 9. Length of first half wave, $\lambda/2$, in bull sperm as a function of viscosity.

Representative waveforms for the bull sperm at the various viscosities are shown in Fig. 10A. The sperm shown at $\eta = 1 \times 10^{-3}$ Pa s^{-1} is identical to the one at 37 °C in Fig. 6A.

EVALUATION OF ACTIVE MOMENTS

This section will investigate what conclusions can be drawn from an estimation of the internal active moments in the bull sperm flagella under the various experimental conditions. The active moments in sperm flagella cannot be directly measured. Rather, they must be calculated, by means of an equation of motion which relates the internal active moments to the flagellar motion.

A brief outline of the calculation methods is first given below. Following this, a determination is made of the active moments which generate (through the equation of motion) simulated flagellar motions resembling as closely as possible the observed

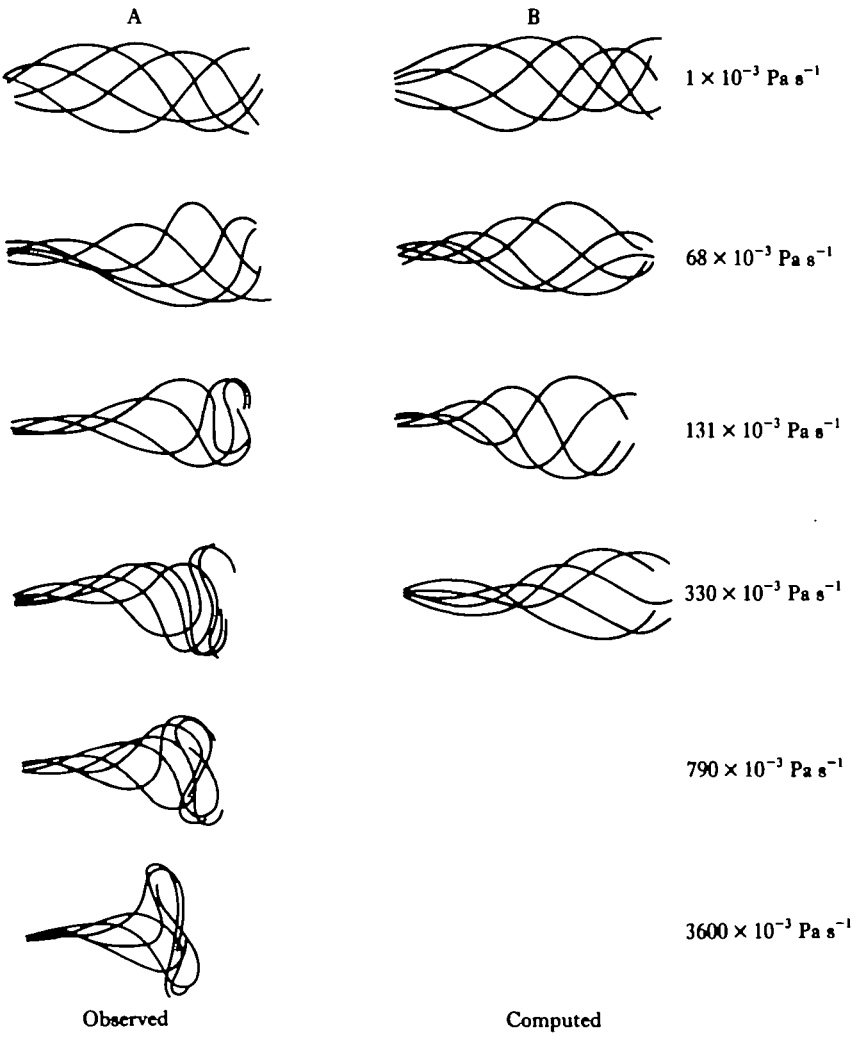

Fig. 10. (A) Typical waveforms of bull sperm in media of raised viscosity. The forward progression of the sperm was removed and the tracings were straightened as explained in Fig. 6A above. (B) Waveforms computed for bull sperm at raised viscosity as explained in the section *Evaluation of active moments*. The waveform at 330×10^{-3} Pa s^{-1} is shown only to illustrate that at this viscosity and higher ones the model calculations did not yield good representations of the observed waveforms.

movements. A model is then developed which explains the active moments in terms of the interaction of dynein and tubulin.

Mathematical techniques

In a sperm flagellum, the moments due to the elastic bending resistance of the flagellar shaft, M_{el}, and those due to the viscous drag in the surrounding fluid, M_{visc}, have to be overcome by the internally produced active moments, M_{act}. This leads to an equation of motion:

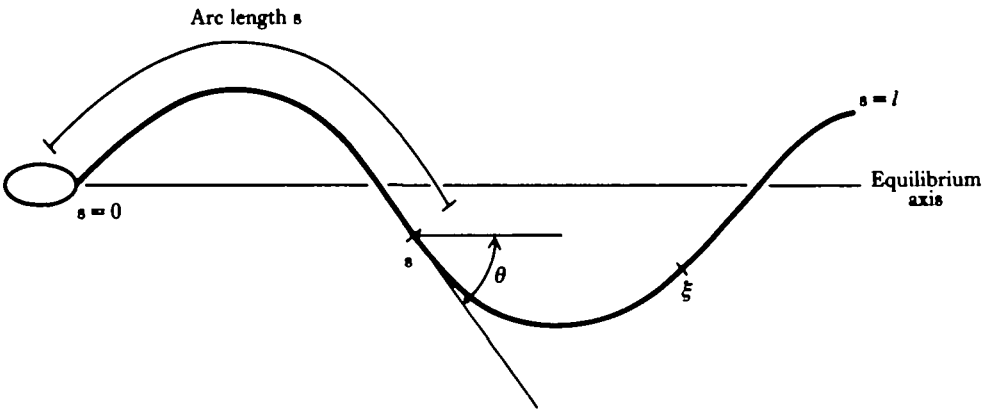

Fig. 11. Coordinate system with the curvilinear distance to the head, s, as the independent coordinate and the angle $\theta(s)$ as the dependent coordinate used in the model calculations. ξ represents a running coordinate along the flagellum.

$$M_{el} + M_{act} = M_{visc} \tag{2}$$

For an accurate evaluation of the terms in equation (2), small amplitude approximations do not suffice (Rikmenspoel, 1978*a*). The large amplitude coordinate system used in the present calculations is illustrated in Fig. 11. The independent variable, s, is the distance measured along the flagellum from the proximal junction, and θ is the dependent variable.

Since the flagellar waves in the bull sperm studied in this paper are planar, it appears reasonable to assume that all moments (when considered as axial vectors) are aligned parallel in a direction perpendicular to the plane of motion. In this section we will proceed taking the above assumption to be true, and consider only the magnitude of the moments.

All segments of the flagellum distal to s contribute to the viscous moment at a location s; the total viscous moment is calculated by integrating the contribution of each elementary segment from s to the end of the flagellum. Since the drag coefficient k_T for tangential motion of a segment is different from that for normal motion k_N, the velocity of the segment has first to be decomposed into tangential and normal components. Multiplying the velocities by the appropriate drag coefficients gives the tangential and normal forces; vector multiplication of the total force by the distance from s to the segment gives the moment contributed by the segment. Full details of the somewhat complex procedure for calculating $M_{visc}(s)$ are set out in Rikmenspoel & Rudd (1973).

The exact expression for the elastic moment M_{el} is

$$M_{el}(s) = IE(s)\frac{1}{\varrho} = IE(s)\frac{\partial\theta}{\partial s} \tag{3}$$

where ϱ is the radius of curvature of the flagellum at s, and IE(s) is the bending resistance (the stiffness) at s. The value of IE(s) is not constant, but it may vary with the location s on the flagellum.

When an expression is found for the internal, active moment M_{act} as a function of

s and of time, equation 2, with equation 3 and the expression for M_{visc}, can be solved by iteration in time. The technique employed for the iteration procedure has been described in detail previously (Rikmenspoel & Rudd, 1973), and it will not be elaborated here. One equation was added in the procedure employed here which represented the condition that the viscous moment at s = 0 should vanish: $M_{visc}(0) = 0$. The model flagellum considered in the calculations below was thus hinged at the proximal junction.

The bull sperm from which the data in the previous section were obtained, were all free at the proximal end. It has been found (Rikmenspoel, 1978*a*), however, that the wave properties of hinged and free bull sperm are virtually identical. Furthermore, the amplitudes of the flagellar waves of the sperm, as shown in Figs 4A and 8A, decrease sharply towards the head in the proximal part of the flagella. An extrapolation of the functions A(s) to the left in Figs 4A and 8A shows that a 'pseudo-hinge point' can be defined for these sperm at approximately $s = -8\,\mu m$. Our computation technique should therefore not lead to serious errors. The advantage of using the same technique as has been employed for cilia (Rikmenspoel & Rudd, 1973) and more recently for sea urchin sperm (Rikmenspoel, 1982) is that values derived here for the active moments in bull sperm are directly comparable to those found previously in cilia and sea urchin sperm.

To find solutions for equation (2) it is necessary to propose a form for the internal active moments, M_{act}, and these moments are not known *a priori*. The procedure followed was to find by trial and error, guided by the results of previous calculations (Rikmenspoel, 1971, 1978*a*, 1982), an expression for M_{act} which led to correct waveforms and wave properties. It should be noted that to derive solutions for the equations of motion it is only required to specify the drag coefficients, k_N and k_T, the stiffness, IE, the active moments, M_{act}, and an initial condition.

Initial calculations

For the normal drag coefficient k_N, the value $k_N = 2{\cdot}1 \times 10^{-7}\,N\,cm^{-2}\,s$ (Rikmenspoel, 1978*a*), derived with the formalism of Gray & Hancock (1955), was used. While refinements to the expression for k_N proposed by Gray & Hancock have been suggested (Lighthill, 1975; Brennen & Winet, 1977), for the present purpose it appears to be adequate (Hiramoto & Baba, 1978). Since the bull sperm flagellum is tapered towards the distal end, a value of k_N decreasing towards the tip should really be used. The dependence of k_N on the flagellar diameter is so weak, however, (Rikmenspoel, 1965) that a constant value of k_N will not cause appreciable errors. The tangential drag coefficient k_T was taken as $k_T = 0{\cdot}5\,k_N$ (Gray & Hancock, 1955).

The midpiece comprises the proximal 12 μm of the flagellum, where the central structure of axoneme and coarse fibres is surrounded by a sheath of mitochondria (Fawcett, 1975 and Fig. 16). A constant value IE_{mp} has been used in the calculations below for the stiffness of the midpiece. The principal part of the flagellum has been approximated as a truncated cone (Rikmenspoel, 1965). The stiffness of the principal piece is then given by $IE(1-s/L)^4$, where L is the extrapolated length of the cone as illustrated in Fig. 12. The expression given above for the stiffness of the principal piece is valid for $12\,\mu m < s < l$. Calculations were performed with a value for l, the total length of the bull sperm flagellum, of $l = 60\,\mu m$ and L, the extrapolated length

of the truncated cone, of L = 90 μm. The adopted values for IE_{mp} and IE were derived as related below.

In cilia, during the effective stroke the internal active moment is developed simultaneously and in phase over the entire length of the cilium (Rikmenspoel & Sleigh, 1970). In the expression for M_{act} during the effective stroke in cilia the location-dependent part and the time-dependent part are thus separated. In those cases where the cilium consists of a single axoneme (e.g. *Paramecium*) the magnitude of the active moment during the effective stroke was found to decrease from the base toward the tip in a linear fashion with the location on the cilium (Rikmenspoel & Rudd, 1973).

Several investigators have concluded that in sperm flagella an active moment occurs which is the equivalent of the active moment during the effective stroke of cilia (Rikmenspoel, 1971, 1978*a*; Phillips, 1972; Brokaw & Goldstein, 1979). Previously made estimates (Rikmenspoel, 1971) of this active moment, called the 'standing moment' because of the absence of a progression along the flagellum, have found it to be decreasing linearly in magnitude towards the tip of the flagellum.

Since the transverse motion of a fixed point on the flagellum is roughly sinusoidal in time, it is natural to assume a sinusoidal variation in time of the standing moment. The above considerations led to an expression for the standing active moment, M_2,

$$M_2 = F(l-s-\delta)\sin \omega t, \tag{4}$$

where $\omega = 2\pi\nu$ is the angular frequency of the flagellar motion; δ represents the length of the inert terminal piece of the flagellum. The shearing force, F, in equation (4) is not dependent on s in a standing moment which decreases linearly with the location s. It should be noted that the magnitude of M_2 in equation (4) at s = 0 is given by $F(l-\delta)$.

Besides the standing moment of equation (4) an active moment is present in flagella which is maximal near the wave crest and which travels along the flagellum with the wave of displacement (Rikmenspoel, 1978*a*; Phillips, 1972). This 'travelling' moment, M_1, is the equivalent of the active moment in cilia during the recovery phase. The travelling moment M_1 can be written, by analogy to equation (1) for the wave of displacement, as

$$M_1 = m(s)\sin[\omega t+\beta(s)]. \tag{5}$$

In equation (5) m(s) expresses the variation of the magnitude of M_1 along the flagellum.

Equations (4) and (5) are valid for $0<s<l-\delta$. In the inert terminal piece, $l-\delta<s<l$, both M_1 and M_2 were taken equal to 0. It was found that computed waveforms were not very sensitive to the exact value of δ. Except where mentioned differently, a value of $\delta = 6\,\mu$m, representing 10% of the total flagellar length, was maintained.

Initial calculations were performed for a model flagellum representing a bull sperm at 37 °C and 1×10^{-3} Pa s^{-1} with a frequency of 20 Hz. The values $IF_{mp} = 3 \times 10^{-17}$ N cm^2 and $IE = 3 \times 10^{-17}$ N cm^2 were used. The function m(s) of equation (5) was taken in these calculations as constant along s, or as decreasing linearly toward the distal end; β(s) was taken as $\beta(s) = (2\pi/\lambda)s$ with λ obtained from the experimental curves as illustrated in Fig. 2B.

When only the travelling moment M_1 was applied (and M_2 was 0), waves in the

model flagellum with a maximum amplitude of 8 μm were obtained when the magnitude of the moment at s = 0 was approximately 2×10^{-14} N cm. The maximum amplitude occurred at a distance of 25–30 μm from the head. More distally, the amplitudes in the model flagella decreased. This decrease was sharper whenever a form of m(s) was used which decreased towards the distal end. When m(s) was taken as constant along the flagellum, the computed amplitude in the distal part (40 μm $< s <$ 60 μm) was approximately one-half of the maximal amplitude at s = 25–30 μm.

When a standing moment M_2 with a magnitude at s = 0 of the order of 3×10^{-14} N cm was applied together with the travelling moment M_1 with a constant m(s), an approximately constant amplitude in the distal half of the flagellum resulted. No combination of a standing moment with a travelling moment which decreased in magnitude towards the distal tip, could be found which yielded wave amplitudes of a more or less constant value in the distal part of the flagellum.

The requirement that the magnitude of the travelling moment, m(s) in equation 5 above, should have a constant value along the flagellum suggests that M_1 is generated by an essentially cylindrical structure, having a constant diameter. The only cylindrical element in the bull sperm flagellum is the axoneme of the nine tubulin-dynein fibres (Fawcett, 1975 and Fig. 16 below). The magnitude of the active moments found above is approximately twice as large as that produced by the axoneme in sea urchin sperm (Rikmenspoel, 1982). With its greater length in bull sperm than in sea urchin sperm (60 μm *versus* 40 μm), and the higher temperature of the bull sperm (37 °C *versus* $\simeq$ 20 °C), the axoneme in bull sperm is likely to be able to provide the active moments required. It should therefore be investigated next what motions would result from the actions of the axoneme alone. Before proceeding to formulate the active moments generated by the axoneme in bull sperm, a few of the parameters of the model used will be fixed to a more definite value.

With the active moments M_1 and M_2 adjusted such that an amplitude of 8 μm (at s = 30 μm) was obtained, waveforms were computed with various values for the stiffness parameters IE_{mp} and IE. The value of the average curvature of the midpiece was obtained from the 'bend angle' $\Delta\theta$, as defined by Gibbons & Gibbons (1980), over the length of the midpiece, Δs. The maximal value of this curvature attained during a flagellar period is shown in Fig. 12 as a function of IE and IE_{mp}. It can be seen in Fig. 12 that the computed curvature of the midpiece depends more strongly on the stiffness of the principal part, defined by IE, than on that of the midpiece itself. This illustrates well the non-local effects of the equations of motion.

The crosshatched band in Fig. 12 shows the range of curvature values measured on the live sperm analysed at 37 °C, 1×10^{-3} Pa s^{-1}. For all calculations below, the values $IE_{mp} = 6 \times 10^{-17}$ N cm^2 and $IE = 3 \times 10^{-17}$ N cm^2 have been adopted. This last value leads to a stiffness of the principal piece at the midpiece junction (s = 12 μm) of $1{\cdot}7 \times 10^{-17}$ N cm^2, close to the values of $1{\cdot}8 \times 10^{-17}$ N cm^2 (Rikmenspoel, 1965) and $1{\cdot}2 \times 10^{-17}$ N cm^2 (Rikmenspoel, Orris & Isles, 1981) found previously from different types of analyses.

A close inspection of Fig. 12 shows that the confidence intervals for the stiffness values adopted above are not narrow and should be $IE_{mp} = (6 \pm 4) \times 10^{-17}$ N cm^2 and $IE = (3 \pm 1) \times 10^{-17}$ N cm^2. Within these confidence intervals, the values are compatible with the stiffness over the whole length of the flagellum ($0 < s < l$) taken as

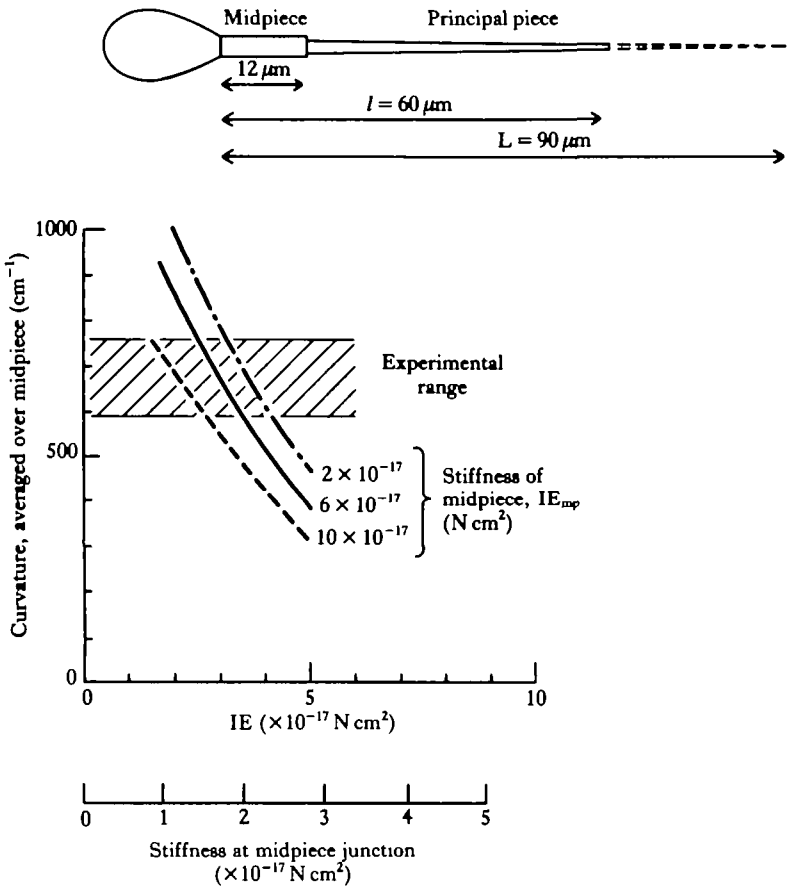

Fig. 12. The curvature, averaged over the length of the midpiece, as a function of the stiffness of the midpiece IE_{mp}, and of the stiffness of the principal piece of the flagellum. The stiffness of the principal piece was taken in the calculations as $IE(1-s/l)^4$. The cross hatched band shows the range of the average curvature of the midpiece measured on the sperm at 37 °C. A diagram of a bull sperm with the tapered principal flagellar piece is shown at the top of the figure.

$IE(s) = 3 \times 10^{-17} \times (1-s/L)^4$ N cm^2. Waveforms computed with an increased constant stiffness in the midpiece appeared to be somewhat smoother, however, than those obtained with a continuously varying stiffness.

The computed waveforms were rather insensitive to the value of L, the extrapolated length of the flagellum, in the range $90\,\mu m < L < 120\,\mu m$. The value $L = 90\,\mu m$ was adopted for all further calculations. With $L = 90\,\mu m$ the stiffness at the distal end of the flagellum, where the axoneme is the only remaining structure, was close to 10^{-18} N cm^2, which is the approximate value of the stiffness of an axoneme (Rikmenspoel & Rudd, 1973; Lindemann, 1975; Brokaw, 1972).

Force-producing model for the axoneme

A detailed model for the active moments produced by the dynein-tubulin interaction

in the axoneme has been developed previously, and has been applied to the motion of cilia (Rikmenspoel & Rudd, 1973) and of sea urchin sperm (Rikmenspoel, 1982). In this model, the axoneme is represented by two sets of microtubules between which dynein cross bridges can form. Dynein bridges on the right side of the axonemal cross section produce positive active moments, while those on the left side yield negative moments.

In a sliding filament mechanism the active moment $M_{act}(s)$ at a location s on the flagellum is made up of the sum of the moments produced by the individual attached dynein cross bridges distal to s. In a previous analysis of ciliary motion (Rikmenspoel, 1976) it was found that during the effective stroke of the cilium of *Sabellaria*, a uniform fraction of the dyneins is attached as cross bridges along the length of the cilium. The active moment then developed per unit length of an axoneme in the cilium of *Sabellaria* was found to be $D = 7{\cdot}2 \times 10^{-12}$ N cm cm^{-1}.

For the present case of an axoneme in a bull sperm flagellum, the active moment $M_{act}(s)$ at a location s on the flagellum can be written as;

$$M_{act}(s) = D \int_s^l f(\xi, t)d\xi, \tag{6}$$

where $f(\xi,t)$ denotes the number of dynein molecules attached as cross bridges at location ξ ($s < \xi < l$) and at time t, normalized to the case of the *Sabellaria* cilium taken as $f(\xi,t) = 1$.

The standing active moment and the travelling active moment in a flagellum must be defined separately, each as a special case of the general expression given in equation (6). The standing moment M_2 is produced by a uniform attachment of dyneins in phase along the flagellum:

$$f(\xi,t) = f_{st} \sin \omega t. \tag{7}$$

The constant f_{st} in equation (7) represents the number of dyneins attached as cross bridges, normalized to that during the effective stroke in the *Sabellaria* cilium taken as 1. f_{st} can be interpreted as the level of activation of the bull sperm axoneme compared to that of the axoneme in *Sabellaria*.

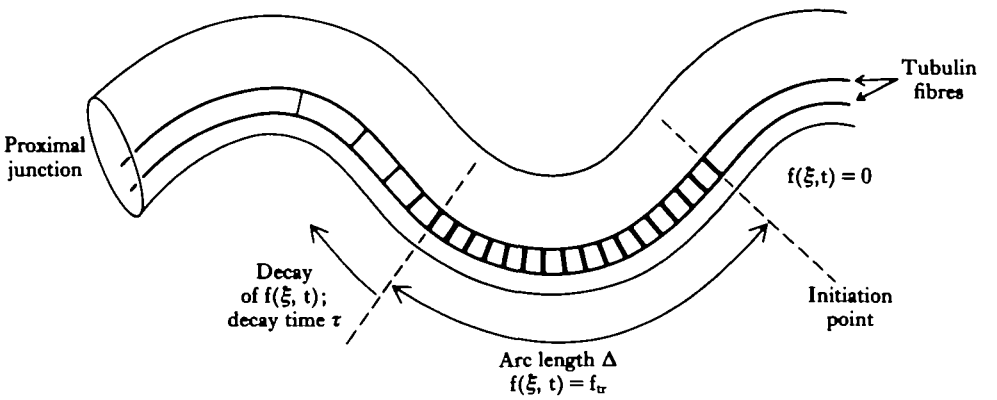

Fig. 13. Diagram illustrating the attachment of dynein cross bridges for the travelling active moment in sperm flagella (courtesy of the Journal of Theoretical Biology).

The travelling moment M_1 occurs as a result of the attachment of dynein cross bridges in the bend sections of the flagella. It is usually thought that the cross bridge attachment is initiated by the development of a bend and the consequent sliding of tubulin fibres relative to each other (Rikmenspoel & Rudd, 1973; Hines & Blum, 1979). Fig. 13 illustrates the formulation used in this paper, which conforms to that used previously for the case of sea urchin sperm flagella (Rikmenspoel, 1982). Distally to an initiation point, no cross bridge attachment occurs. Over an arc length, Δ, proximal to the initiation point, the dynein attachment is at a constant level: $f(\xi,t) = f_{tr}$. Proximally to the bend the dynein attachment decays exponentially with a decay time τ. In all calculations below, a value of $\Delta = 12\,\mu$m, representing slightly less than one-quarter of the wavelength, and a decay time $\tau = 5$ ms were maintained. It has been found previously (Rikmenspoel, 1982) that computed waveforms are not very sensitive to the precise values of Δ and τ. The progression velocity v of the initiation point was taken as $v = \nu\lambda$, with λ obtained from the data in Figs 5 and 9.

The total active moment M_{act} is the sum of the standing moment M_2 and the travelling moment M_1. Since in the sperm flagella several curved sections were always present, usually two to three partially overlapping travelling moment sequences (with alternating signs) had to be computed at each instant.

With the above formulation for the dynein-tubulin interaction in the axoneme, the model for computing waveforms was in fact completely fixed. The only uncommitted variables were the activation parameters f_{st} and f_{tr} for the standing and the travelling moments. It should furthermore be noted that the computation technique was identical to that used recently in obtaining waveforms and active moments in sea urchin sperm flagella (Rikmenspoel, 1982).

In the actual calculations described below, the initial position was always a straight flagellum. The travelling and the standing moment were applied with a relative phase determined by trial and error to result in the smoothest waveform. A steady state motion of the model flagellum was reached during the second cycle of motion. All waveforms and wave properties reported below were from the third or fourth cycle of motion after the start of the calculation.

When only the travelling moment was applied (and thus $f_{st} = 0$) to a model flagellum with a frequency $\nu = 20$ Hz, the computed flagellar waves showed an amplitude at $s = 30\,\mu$m of approximately $8\,\mu$m for a value of $f_{tr} = 1{\cdot}2$. In the distal part of the flagellum, the computed wave amplitude was lower than that observed on live sperm at 37 °C and 1×10^{-3} Pa s^{-1}, as illustrated by the dotted line in Fig. 14. When a properly phased, standing moment was applied ($f_{st} \neq 0$) together with the travelling moment, the amplitude of the computed waves in the distal part was increased, as shown in Fig. 14.

The best fit of the computed amplitudes with the data was obtained with $f_{st} = 1{\cdot}0$. For higher values of f_{st} the amplitudes for $s > 40\,\mu$m decreased slowly and the shapes of the computed waves deteriorated. The value $f_{st} = 1{\cdot}0$, with a probable error of perhaps 20 %, was therefore adopted.

The magnitudes of the travelling, standing and total active moments in the model flagellum at 20 Hz, representing the 'control' sperm at 37 °C and 1×10^{-3} Pa s^{-1}, are shown in Fig. 15A. Due to the changing phase difference along the flagellum between the standing and the travelling moment, the total moment varies rather irregularly.

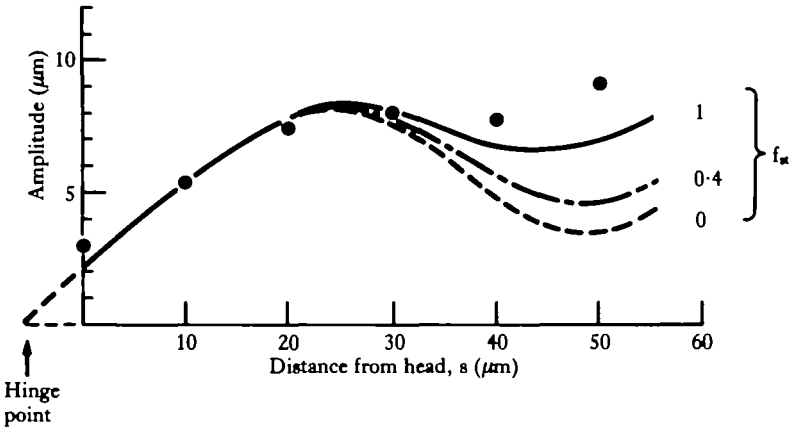

Fig. 14. Amplitude as a function of the distance to the head, s, computed for a bull sperm at 37 °C in which the axoneme alone powered the motility. The dots are the experimental values taken from Fig. 4A. The curves were computed with different values of the standing moment, represented by the activation parameter f_{st} as shown. The computed curves were shifted slightly to the left to make the hinge point in the model coincide with the 'pseudo-hinge point' of the live sperm as explained in the text.

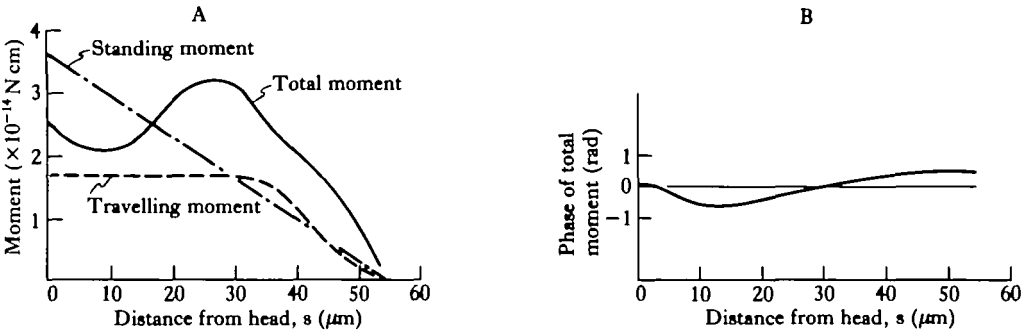

Fig. 15. (A) Magnitude of the travelling, the standing and the total (= travelling + standing) active moments in bull sperm at 37 °C, as a function of the distance from the head, s. (B) Phase of the total active moment, relative to the phase at the head junction, as a function of the distance from the head, s.

The phase of the total moment relative to that at the proximal junction is shown as a function of the distance along the flagellum, s, in Fig. 15B. It can be seen in Fig. 15B that the total active moment shows phase differences of at most 1 rad over the length of the flagellum.

A computed waveform at $f_{st} = 1{\cdot}0$ and $f_{tr} = 1{\cdot}2$ for a sperm at 20 Hz is shown in Fig. 6B above in the Results section. Even though small differences are apparent, the computed waveshape represents the observed shape rather well.

The same procedure as outlined above for sperm at 37 °C was followed to obtain waveshapes and active moments in the sperm at lower temperatures. First, f_{tr} was adjusted so that the amplitude in the middle of the flagellum corresponded to that observed in the live sperm. The value of f_{st} which gave the best fit of the variation of amplitude along the flagellum was then determined. The wave amplitudes thus computed are inserted in Fig. 4A above, for model sperm at 37, 11 and 5 °C. It can be seen in Fig. 4A that at lower temperatures (11 and 5 °C) the variation of amplitude along the flagellum in live sperm is quite well reproduced in the model flagella.

Table 1. *Activation parameters f_{tr} and f_{st} for the travelling and the standing active moments in bull sperm in the temperature range 37 to 5 °C*

Temperature (°C)	Average frequency (Hz)	f_{tr}	f_{st}	$\bar{M}_t$ (s = 0) N cm	$\bar{M}_s$ (s = 0) N cm
37	20·5	1·2	1·0	$1{\cdot}7 \times 10^{-14}$	$3{\cdot}6 \times 10^{-14}$
28	12·5	0·9	0·8	$1{\cdot}2 \times 10^{-14}$	$2{\cdot}6 \times 10^{-14}$
20	6·1	0·5	0·4	$0{\cdot}61 \times 10^{-14}$	$1{\cdot}4 \times 10^{-14}$
11	3·3	0·25	0·22	$0{\cdot}29 \times 10^{-14}$	$0{\cdot}74 \times 10^{-14}$
5	1·1	0·06	0·05	$0{\cdot}07 \times 10^{-14}$	$0{\cdot}17 \times 10^{-14}$

The magnitudes of the corresponding travelling moment, $\bar{M}_t$, and standing moment, $\bar{M}_s$, at the head junction (s = 0) are also shown.

Table 1 summarizes the values for f_{tr} and f_{st} obtained for bull sperm at the various temperatures in the range 37–5 °C. It is worth noting that the values of f_{tr} and f_{st} in bull sperm at 20 °C (0·5 and 0·4 respectively) are close to the values $f_{tr} = 0{\cdot}6$ and $f_{st} = 0{\cdot}4$ reported recently for sea urchin sperm at a comparable temperature of 22 °C. Inserted in Table 1 are the values for the travelling and the standing active moments at the proximal junction (s = 0).

In Fig. 6B in the Results section, the computed waveforms at the various temperatures are shown. A comparison with the tracing of the live sperm in Fig. 6A shows that at all temperatures the active moments produced in the axoneme of the flagella lead to computed waveforms quite similar to the observed ones.

At raised viscosity it proved necessary to increase the values of f_{tr} and f_{st} to obtain computed wave amplitudes comparable to those observed in live sperm. The same procedure for fitting computed waveshapes to those observed on live sperm was used as described above for the temperature dependence measurements. It was found that at the high viscosities, the application of a travelling moment alone resulted in a maximum amplitude in the distal part of the model flagella at $s \simeq 40$–$50\,\mu m$. The amplitude in the proximal part, $s = 10$–$20\,\mu m$, was comparatively too high. The addition of a standing moment depressed the amplitude in the proximal part while showing little effect on the wave in the distal part of the model flagellum.

Waveforms somewhat analogous to the observed ones in live sperm could be computed for viscosities of 68 and 131×10^{-3} Pa s^{-1}. These waveforms are shown in Fig. 10B above in the Results section. It can be seen in Fig. 10B that in the distal part the wave in the model flagella at 68 and 131×10^{-3} Pa s^{-1} travels more slowly than that in the live sperm. This reflects the fact that the curvature of the function $\alpha(s)$ has been neglected in the calculations (compare Fig. 2B above). The computed waveforms at viscosities of 330×10^{-3} Pa s^{-1} and higher were poor. In Fig. 10B above, the model waveshape at 330×10^{-3} Pa s^{-1} is shown only to illustrate that at these extreme viscosities, the use of a constant travelling velocity of the flagellar wave [represented by a straight form of the function $\alpha(s)$] results in a computed wave which travels too fast in the proximal part and too slowly in the distal part of the flagellum. Even though accurate waveforms could not be obtained at 300, 790 and 3600×10^{-3} Pa s^{-1}, an approximate determination of f_{tr} and f_{st} was made by fitting computed wave

Table 2. *Activation parameters f_t and f_s for the travelling and the standing active moments in bull sperm at 37 °C, as a function of viscosity, η*

Viscosity $\times 10^{-3}$ Pa s^{-1}	Average frequency (Hz)	f_{tr}	f_{st}	$\bar{M}_t$ ($s = 0$) (N cm)	$\bar{M}_s$ ($s = 0$) (N cm)
1	20·5	1·2	1·0	$1{\cdot}7 \times 10^{-14}$	$3{\cdot}6 \times 10^{-14}$
68	3·0	8·0	6·0	$9{\cdot}1 \times 10^{-14}$	$1{\cdot}9 \times 10^{-13}$
131	2·2	10·4	8·0	$1{\cdot}7 \times 10^{-13}$	$2{\cdot}6 \times 10^{-13}$
360	1·67	18	15	$2{\cdot}1 \times 10^{-13}$	$4{\cdot}9 \times 10^{-13}$
790	1·03	18	15	$2{\cdot}1 \times 10^{-13}$	$4{\cdot}9 \times 10^{-13}$
3600	0·45	28	23	$3{\cdot}1 \times 10^{-13}$	$7{\cdot}7 \times 10^{-13}$

The magnitudes at $s = 0$ of the corresponding travelling moment, $\bar{M}_t$, and standing moment, $\bar{M}_s$, are also shown. All values for viscosities $\eta > 131 \times 10^{-3}$ Pa s^{-1} are estimates (more probably upper limits) as explained in the text.

amplitudes as outlined above. Table 2 shows the values of f_{tr} and f_{st} as well as the values for the corresponding active moments obtained at the various viscosities in the range $1–3600 \times 10^{-3}$ Pa s^{-1}.

In Fig. 10A above it can be observed that at the highest viscosities the distal part of the live sperm tends to slide in a tangential fashion through the fluid. In the computed sperm the motion was largely normal to the flagellum, however. Since the normal drag coefficient is twice the tangential one, the viscous drag, and thereby the active moments necessary to overcome it, are overestimated in the model flagella by perhaps as much as a factor of two. The values of f_{tr}, f_{st}, M_1 and M_2 in Table 2 should therefore be considered as upper limits, with the probable values, especially for the highest viscosities, a factor of two lower than those shown.

DISCUSSION

The results of the calculations above show that in the temperature range of 5–37 °C, the axoneme in bull sperm flagella can, by itself, produce sufficient active moment to power the motility. For bull sperm at 37 °C, the amount of active moment per unit length of axoneme was found to be almost identical to that in the *Sabellaria* cilium (Rikmenspoel & Rudd, 1973). This can be seen in Table 1 above where the 'activation parameters' f_{tr} and f_{st} (with values of 1·2 and 1·0, respectively) were normalized to the *Sabellaria* cilium taken as 1. For sea urchin sperm flagella values of $f_{tr} = 0{\cdot}6$ and $f_{st} = 0{\cdot}4$ were recently reported (Rikmenspoel, 1982). These values applied to sea urchin sperm at a temperature of 22 °C. For bull sperm at 20 °C, Table 1 shows almost identical values of $f_{tr} = 0{\cdot}5$ and $f_{st} = 0{\cdot}4$. This indicates that at the same temperature the amount of active moment per dynein molecule in the two species (compare equation 6 above) is practically equal. It should be noted that since the same calculation technique was used for the sea urchin sperm and for the bull sperm, these conclusions should not be model dependent.

At very high viscosity the values derived for f_{tr} and f_{st} varied from 15 to 28, as shown in Table 2. It could be questioned whether the axoneme can indeed increase its force production by such a factor above that occurring at normal viscosity. In the subsection

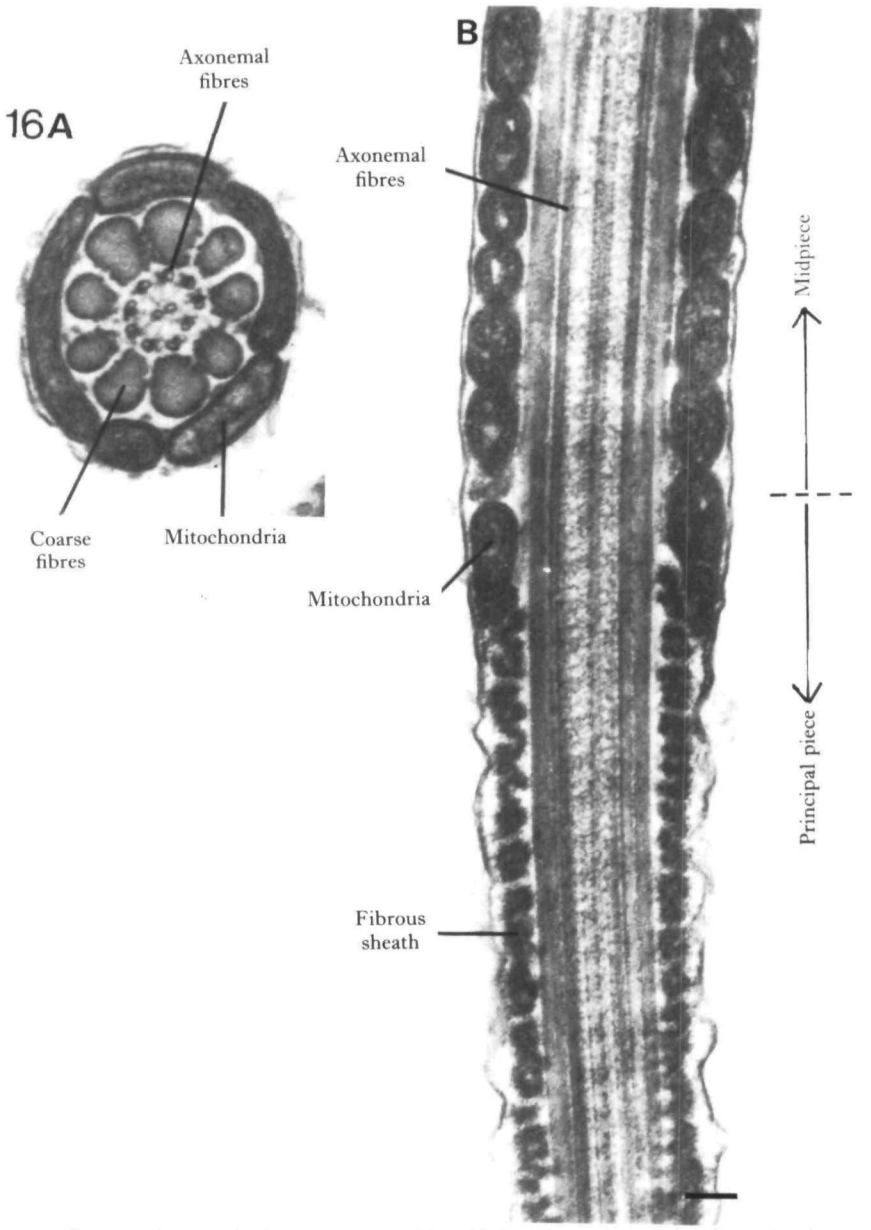

Fig. 16. (A) Electron micrograph of a cross section of the midpiece of a bull sperm flagellum, showing the axonemal inner fibres, the coarse fibres, and the mitochondrial sheath surrounding the coarse fibres (courtesy of the Biophysical Journal). (B) Longitudinal section of a bull sperm flagellum in the area of the midpiece junction. The coarse fibres do not show a discontinuity at this junction. The changeover from a mitochondrial sheath in the midpiece to the fibrous sheath in the principal piece can be seen (courtesy of Mrs Sandra Orris). Calibration bar = 0·1 μm.

Force-producing model for the axoneme it was shown, however, that the estimates for f_{tr} and f_{st} at viscosities above 300×10^{-3} Pa s^{-1} are probably too high by at least a factor of two.

Using the same mathematical formalism as was employed in this paper, a value for the activation parameters of approximately 12 has been reported for the cilia of the organism *Phragmatopoma* (Rikmenspoel, 1976), at a high external viscosity. For the case of cilia, in which each movement phase stands by itself and can be uniquely interpreted, the calculation procedures should be very good. Therefore, the large value of the activation parameters in *Phragmatopoma* at high viscosity, representing a more than 20-fold increase over the value at normal viscosity, should not be in doubt. In the sperm of the annelid *Chaetopterus* at raised viscosity (14×10^{-3} Pa s^{-1}), a value of $f_{tr} = 8$ was found recently (Rikmenspoel, 1982), again using the same calculation procedure. There was no indication that this represented a limit.

As stated above, the probable values for f_{tr} and f_{st} in bull sperm at the highest viscosities are in the order of 10 to 15, not much above those occurring in the axonemes of *Phragmatopoma* cilia and *Chaetopterus* sperm. It appears, therefore, that the axoneme is indeed capable of powering the movements of bull sperm flagella over the whole range of viscosities used in this paper, and that no other force-producing structures are required.

It would be desirable to have precise determinations of f_{tr} and f_{st} in bull sperm at very high viscosities. To this end it would be necessary to refine the model calculations used by introducing a variable travelling velocity of the waves, and possibly other location-dependent parameters as well. This kind of detailed modelling, which would essentially be a curve fitting procedure, is outside the scope of this paper.

In the subsection *Initial calculations* it was found that computed flagellar waves with an increasing amplitude towards the distal end could only be obtained with a travelling moment of at least constant (not diminishing) magnitude along the flagellum. The simplest explanation, though not the only possible one, for this finding is that the structure producing the active moment has constant dimensions over the length of the flagellum. Since the axoneme is the only cylindrical structure in the bull sperm flagellum, our results thus suggest that no other force-producing mechanism besides the axoneme is operating in these flagella. In particular, the coarse fibres are likely to have only a passive role.

All of the above considerations have been based on the observations in this paper which were made on bull spermatozoa with a flat, two-dimensional, tail wave. Caution should, therefore, be exercised in extrapolating the conclusions to bull spermatozoa displaying helical, three-dimensional waves. On purely intuitive grounds, it seems unlikely, however, that the coarse fibres would have an active, force-producing function only in the case of helical flagellar waves.

Phillips (1972) proposed that the coarse fibres in mammalian sperm provide the stiffness against bending for the flagella. The presence of keratin-like proteins in the coarse fibres (Baccetti *et al.* 1976; Price, 1973) would support this. A simple calculation given below indicates that the coarse fibres can indeed be the site in which all of the flagellar stiffness resides.

Fig. 16A shows a cross section of the midpiece of a bull sperm flagellum. It has been found in this paper that the stiffness at this location $IE_{mp} = 6 \times 10^{-17}$ N cm^2. In the

expression for the stiffness I is defined as $\int r^2 d\sigma$, where $d\sigma$ is an element of the cross section of the flagellum and r is the distance of the element $d\sigma$ to the median plane. The integral is to be taken over the cross section. The average diameter of the coarse fibres in Fig. 16A is $0{\cdot}1\ \mu m = 10^{-5}$ cm. With a distance r for the coarse fibres varying from $0{\cdot}075\ \mu m = 7{\cdot}5 \times 10^{-6}$ cm to $0{\cdot}15\ \mu m = 1{\cdot}5 \times 10^{-5}$ cm, the value of I for all the coarse fibres is $I = 1{\cdot}2 \times 10^{-19}\,cm^4$. The value of the Young's Modulus, E, of the coarse fibres necessary to obtain a stiffness of the midpiece of the flagellum $IE = 6 \times 10^{-7}$ is thus $E = 5 \times 10^2\,N\,cm^{-2}$. This is well within the range of values for E of protein-based biological materials (Yamada, 1970). The coarse fibres can, therefore, indeed provide all of the stiffness of the midpiece of bull sperm flagella. It can easily be ascertained that this is also the case in the principal piece of the flagellum.

In an earlier analysis of the stiffness of the bull sperm flagellum (Rikmenspoel, 1965) a value of $I \simeq 4 \times 10^{-21}\,cm^4$ at the midpiece junction (at $s = 12\ \mu m$) was used. This estimate was based on the much less detailed electron microscopic evidence of the flagellar structure available then. Essentially the same value of the stiffness at the midpiece junction of $1{\cdot}8 \times 10^{-17}\,N\,cm^2$ was derived in the earlier paper as that found presently of $1{\cdot}7 \times 10^{-17}\,N\,cm^2$ (see Fig. 12 above). However, the earlier conclusion that the coarse fibres would have to possess a Young's Modulus E of $\simeq 4 \times 10^3\,N\,cm^2$ to cause all of the stiffness of the flagellum needs to be corrected, as stated above.

In the principal piece of the bull sperm flagellum, the mitochondrial sheath surrounding the coarse fibres is replaced by a fibrous sheath consisting of ring-like structures as illustrated in Fig. 16B. The function of this fibrous sheath could well be to provide a mechanical restraint on the coarse fibres, preventing radial movement. It should be kept in mind that the equivalent of the radial spokes and nexin links which bind the axonemal fibres into an integral structure (Stephens, 1974) is absent for the coarse fibres. The fibrous sheath could thus act analogously to the rings on a barrel.

The experimental data in this paper make it possible to estimate the amount of mechanical work performed by bull sperm as a function of temperature. Taylor (1952) has derived the work, W, performed by a sperm flagellum against the viscous drag in the surrounding fluid as:

$$W = \frac{4\pi^3 \eta \nu^2 b^2 l}{0{\cdot}62 - \ln \frac{2\pi a}{\lambda}}, \tag{8}$$

where b is the average amplitude of the flagellar wave and a is the radius of the flagellar cross section. Carlson (1962) has shown that the hydrodynamic work as given in equation (8) is not model dependent. The derivation of equation (8) was done in small amplitude approximation. In evaluating W, the value of the wavelength, measured along the equilibrium axis of the sperm, $\lambda(x)$, was therefore used.

Table 3 shows the amount of hydrodynamic work calculated with equation (8) and using the data from the Results section. Inserted in Table 3 is the hydrodynamic work performed by sea urchin spermatozoa at 16–22 °C, derived from the data of Brokaw (1966) and Rikmenspoel (1978*b*). No corrections were applied for the work done by the sperm in the elastic deformation of the flagella since this elastic work would at most be 1/3 of the hydrodynamic work (Machin, 1958). Table 3 shows that for bull spermatozoa the amount of work performed drops precipitously with the temperature. A

Table 3. *Mechanical work, W, performed per sperm against the viscous drag of the surrounding fluid for bull sperm at temperatures ranging from 37 to 5 °C, and for sea urchin sperm at 16–22 °C*

Species	Temperature (°C)	υ (Hz)	b (μm)	$\lambda(x)$ (μm)	W ($J\,s^{-1}$ $sperm^{-1}$)
Bull	37	20·5	8·0	54	$4{\cdot}5 \times 10^{-14}$
	28	12·5	7·5	56	$1{\cdot}5 \times 10^{-14}$
	20	6·1	5·2	56	$1{\cdot}7 \times 10^{-15}$
	11	3·3	4·8	64	$3{\cdot}9 \times 10^{-16}$
	5	1·1	3·0	92	$1{\cdot}6 \times 10^{-17}$
Sea urchin	16–22	30	4·0	22	$2{\cdot}1 \times 10^{-14}$

The work was calculated according to the formula of Taylor (1952), equation 10 of the text. The values for the average flagellar frequency, υ, amplitude, b, and wavelength measured along the x axis, $\lambda(x)$, are also shown. The data for bull sperm were from the experiments in this paper, those for sea urchin from Brokaw (1966) and Rikmenspoel (1978).

a temperature of 20 °C, the work performed by a bull sperm proves to be roughly an order of magnitude less than that by sea urchin sperm at a comparable temperature of 16–22 °C.

At the physiological temperature for bull sperm, 37 °C, the hydrodynamic work per sperm is slightly more than twice that of sea urchin sperm at 16–22 °C. Normal bull spermatozoa show a helical flagellar wave, with each component contributing to the work performed (Rikmenspoel *et al.* 1969). The greater stiffness of the bull sperm compared to invertebrate sperm causes the work required for elastic deformation to be larger for bull sperm. The combined effects of these corrections would be to bring the total amount of work performed by a bull sperm at 37 °C to about three to four times that of a sea urchin sperm at 16–22 °C. This ratio is close to that of the ATP turnover for the two species mentioned in the Introduction.

The axoneme of a bull sperm contains, with a length of 60 μm and a spacing between successive dynein pairs on each tubulin fibre of 17 nm, a total of $6{\cdot}5 \times 10^4$ dynein molecules. A sea urchin sperm with a length of 40 μm contains in total $4{\cdot}3 \times 10^4$ dynein molecules. Thus for the bull sperm at 37 °C the amount of hydrodynamic work per dynein molecule is equal to 7×10^{-19} $J\,s^{-1}$ $dynein^{-1}$, and for sea urchin sperm at 16–22 °C is 5×10^{-19} $J\,s^{-1}$ $dynein^{-1}$. At their physiologically optimal temperatures, the dyneins in the two species perform, therefore, a comparable amount of hydrodynamic work. After corrections for the elastic work and, in bull sperm, for the effects of a helical wave, the total work normalized per dynein molecule can be expected to be 2 to 2·5 times higher in a rotating bull sperm at 37 °C than in a sea urchin sperm at 16–22 °C. With the different temperatures for the two species this appears not to present a conflict. At all temperatures below 37 °C, the work per dynein molecule in a bull sperm is actually lower than in sea urchin sperm at 16–22 °C, as can readily be derived with the aid of Table 3.

Some of the experimental findings in this paper are of interest. It was found (see Fig. 7) that over the wide range of viscosities, η, of $1\text{–}3600 \times 10^{-3}$ $Pa\,s^{-1}$, the frequency, ν, of the bull sperm motion varied as $\nu \propto \eta^{-1/2}$. This means that models

in which expressions for the flagellar frequency are derived (compare Hines & Blum 1979; Brokaw & Rintala, 1974) have to incorporate mechanochemical feedback mechanisms which explain this simple viscosity dependence.

In *Crithidia* and in the sperm of *Lythechinus* and *Chaetopterus* a decrease in the flagellar frequency proportional to η^{-p} ($p \approx 0{\cdot}25$–$0{\cdot}3$) occurs in the range $1 < \eta < 40 \times 10^{-3}\,Pa\,s^{-1}$ (Coakley & Holwill, 1974; Brokaw, 1966). The amplitude of the flagellar motion in *Lythechinus* decreases strongly, whereas in *Chaetopterus* it appears constant at high viscosity (Brokaw, 1966). Apparently, species differences occur in the mechanochemical feedback of the external fluid onto the flagellar motion. This might necessitate the development of species-specific models.

At high viscosity, the motion of the head of bull sperm and the transverse movement of the flagellum near the head become very small as shown in Figs 8 and 10 above. The sperm in these experiments are free swimming and not attached to the microscope slide. This observation indicates that in refined models for the active moments which can generate accurate waveforms at the highest viscosities, the influence of the forces on the sperm head probably cannot be neglected.

As a function of temperature, the flagellar frequency was found to show a straight Arrhenius plot in the range 37–11 °C, with a Q_{10} of 2·1. The active travelling and standing moments of Table 1 were plotted according to Arrhenius in Fig. 17. Even though a slight curvature is present in Fig. 17, both the travelling and the standing moments show the same Q_{10} of 2·1 as the flagellar frequency in Fig. 3B. The flagellar

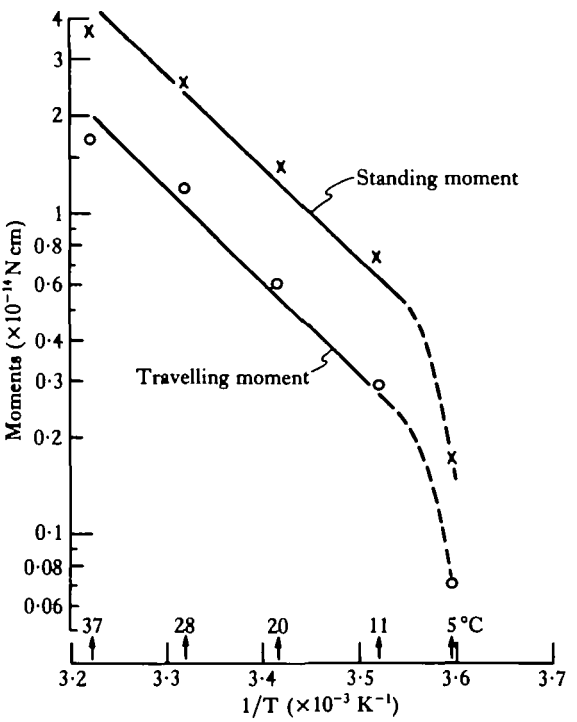

Fig. 17. Arrhenius plot of the travelling and the standing active moment in bull sperm as a function of temperature. The lines were drawn by eye.

frequency and the amount of active moment developed thus appear each to be dominated by a single rate constant. It is not necessarily the same rate constant which dominates both, however.

I wish to thank Alice Jacklet for the cinemicrography in the experiments in this paper, Ulrika Schaal for the analysis of the films and Cheryl Isles for reading the manuscript. This investigation was supported by the National Science Foundation through Grant PCM-803700.

REFERENCES

BACCETTI, B., PALLINI, V. & BURRINI, A. G. (1973). The accessory fibers of the sperm tail. I. Structure and chemical composition of the bull "coarse fibers". *J. submic. Cytol.* **5**, 237–256.

BACCETTI, B., PALLINI, V. & BURRINI, A. G. (1976). The accessory fibers of the sperm tail. III. High-sulfur and low-sulfur components in mammals and cephalopods. *J. Ultrastruct. Res.* **57**, 289–308.

BRENNEN, C. & WINET, H. (1977). Fluid mechanics of propulsion by cilia and flagella. *Ann. Rev. Fluid Mech.* **9**, 339–398.

BROKAW, C. J. (1966). Effects of increased viscosity on the movements of some invertebrate spermatozoa. *J. exp. Biol.* **45**, 113–139.

BROKAW, C. J. (1972). Computer simulation of flagellar movement. II. Influence of external viscosity on the movement of the sliding filament model. *J. mechanochem. Cell Mot.* **1**, 203–211.

BROKAW, C. J. & BENEDICT, B. (1968). Mechanochemical coupling in flagella. II. Effects of viscosity and thiourea on metabolism and motility of *Ciona* spermatozoa. *J. gen. Physiol.* **52**, 283–299.

BROKAW, C. J. & GOLDSTEIN, S. F. (1979). Asymmetrical oscillations of sea urchin sperm flagella induced by calcium. In *The Spermatozoon*, (ed. D. W. Fawcett). Baltimore, Munich: Urban & Schwarzenberg Inc.

BROKAW, C. J. & JOSSLIN, R. (1973). Maintenance of constant wave parameters by sperm flagella at reduced frequencies of beat. *J. exp. Biol.* **59**, 617–628.

BROKAW, C. J. & RINTALA, D. R. (1974). Computer simulation of flagellar movement. III. Models incorporating crossbridge kinetics. *J. mechanochem. Cell Mot.* **3**, 77–86.

BURNASHEVA, S. A. (1958). Properties of spermosin, a contractile protein, in sperm cells. *Biokhimiya* **23**, 558–563.

CARLSON, F. D. (1962). A theory of the survival value of motility. In *Spermatozoan Motility*, (ed. D. W. Bishop), pp. 137–146. AAAS, Washington, D.C.

COAKLEY, C. J. & HOLWILL, M. E. J. (1974). Effects of pressure and temperature changes on the flagellar movement of *Crithidia oncopelti*. *J. exp. Biol.* **60**, 605–629.

ENGELHARDT, V. A. & BURNASHEVA, S. A. (1957). Localization of the protein spermosinin sperm cells. *Biokhimiya* **22**, 513–518.

FAWCETT, D. W. (1975). The mammalian spermatozoon. *Devl Biol.* **44**, 394–436.

FRIEND, D. S., ELIAS, P. M. & RUDOLF, I. (1979). Disassembly of the guinea pig sperm tail. In *The Spermatozoon*, (eds D. W. Fawcett & J. M. Bedford), pp. 157–168. Baltimore, Munich: Urban & Schwarnenberg Inc.

GIBBONS, I. R. & GIBBONS, B. H. (1980). Transient flagellar waveforms during intermittent swimming in sea urchin sperm. I. Wave parameters. *J. Muscle Res. Cell Mot.* **1**, 31–59.

GRAY, J. & HANCOCK, G. J. (1955). The propulsion of sea urchin spermatozoa. *J. exp. Biol.* **32**, 802–814.

HINES, M. & BLUM, J. J. (1979). Bend propagation in flagella. II. Incorporation of dynein cross bridge kinetics into the equations of motion. *Biophys. J.* **25**, 421–442.

HIRAMOTO, Y. & BABA, S. A. (1978). A quantitative analysis of flagellar movement in echinoderm spermatozoa. *J. exp. Biol.* **76**, 85–104.

LIGHTHILL, M. J. (1975). *Mathematical Biofluid Dynamics*. Philadelphia: S.I.A.M.

LINDEMANN, C. B. (1975). An analytical measurement of the stiffness of intact and demembranated sea urchin sperm during motility. *Biophys. J.* **15**, 160a (Abstract).

LINDEMANN, C. B. & GIBBONS, I. (1975). Adenosine triphosphate induced motility and sliding filaments in mammalian sperm extracted with Triton X-100. *J. Cell Biol.* **65**, 147–162.

LINDEMANN, C. B. & RIKMENSPOEL, R. (1972). Simple viscometer for samples less than 1 ml. *J. sci. Instr.* **5**, 178–180.

LINDEMANN, C. B., RUDD, W. G. & RIKMENSPOEL, R. (1973). The stiffness of the flagella of impaled bull sperm. *Biophys. J.* **13**, 437–448.

MACHIN, K. E. (1958). Wave propagation along flagella. *J. exp. Biol.* **35**, 796–806.

NELSON, K. (1962). Cytochemical aspects of spermatozoan motility. In *Spermatozoan Motility*, (ed. D. W. Bishop), pp. 171–188. Washington, D.C.: AAAS.

NEVO, A. C. & RIKMENSPOEL, R. (1970). Diffusion of ATP in sperm flagella. *J. theor. Biol.* **26**, 11–18.

NICHOLS, K. N. & RIKMENSPOEL, R. (1977). Mg^{2+}-dependent electrical control of flagellar activity in *Euglena*. *J. Cell Sci.* **23**, 211–225.

O'DAY, P. M. & RIKMENSPOEL, R. (1979). Electrical control of flagellar activity in impaled bull spermatozoa. *J. Cell Sci.* **35**, 123–138.

PATE, E. F. & BROKAW, C. J. (1980). Movement of spermatozoa in viscous environments. *J. exp. Biol.* **88**, 395–397.

PHILLIPS, D. M. (1972). Comparative analysis of mammalian sperm motility. *J. Cell Biol.* **53**, 561–573.

PIHLAJA, D. J. & ROTH, L. E. (1973). Bovine sperm fractionation. II. Morphology and chemical analysis of tail segments. *J. Ultrastruct. Res.* **44**, 293–309.

PRICE, J. M. (1973). Biochemical and morphological studies of outer dense fibers of rat spermatozoa. *J. Cell Biol.* **59**, 272a (Abstract).

RIKMENSPOEL, R. (1957). An optically clear egg-yolk diluent for bull spermatozoa. *Experientia* **13**, 124–125.

RIKMENSPOEL, R. (1965). The tail movement of bull spermatozoa. Observations and model calculations. *Biophys. J.* **5**, 365–392.

RIKMENSPOEL, R. (1971). Contractile mechanisms in flagella. *Biophys. J.* **11**, 446–463.

RIKMENSPOEL, R. (1976). The contractile events in the cilia of *Paramecium, Opalina, Phragmatopoma* and *Mytilus*. *Biophys. J.* **16**, 445–473.

RIKMENSPOEL, R. (1978*a*). The equation of motion for sperm flagella. *Biophys. J.* **23**, 177–206.

RIKMENSPOEL, R. (1978*b*). Movement of sea urchin sperm flagella. *J. Cell Biol.* **76**, 310–322.

RIKMENSPOEL, R. (1982). Ciliary contractile model applied to sperm flagellar motion. *J. theor. Biol.* **96**, 617–645.

RIKMENSPOEL, R., VAN HERPEN, G. & EYKHOUT, P. (1960). Cinematographic observations of the movements of bull sperm cells. *Physics Med. Biol.* **5**, 167–181.

RIKMENSPOEL, R., JACKLET, A. C., ORRIS, S. E. & LINDEMANN, C. B. (1973). Control of bull sperm motility. Effects of viscosity, KCN and thiourea. *J. mechanochem. Cell Mot.* **2**, 7–24.

RIKMENSPOEL, R., ORRIS, S. E. & ISLES, C. A. (1981). Effects of vanadate, Mg^{2+} and electric current injection on the stiffness of impaled bull spermatozoa. *J. Cell Sci.* **51**, 53–61.

RIKMENSPOEL, R. & RUDD, W. G. (1973). The contractile mechanism in cilia. *Biophys. J.* **13**, 955–993.

RIKMENSPOEL, R., SINTON, S. & JANICK, J. J. (1969). Energy conversion in bull sperm flagella. *J. gen. Physiol.* **54**, 782–805.

RIKMENSPOEL, R. & SLEIGH, M. A. (1970). Bending moments and elastic constants in cilia. *J. theor. Biol.* **28**, 81–100.

STEPHENS, R. E. (1974). Enzymatic and structural proteins of the axoneme. In *Cilia and Flagella*, (ed. M. A. Sleigh). London, New York: Academic Press.

SUMMERS, K. & GIBBONS, I. R. (1971). Adenosine triphosphate induced silding of tubules in trypsin treated flagella of sea urchin sperm. *Proc. natl Acad. Sci. U.S.A.* **68**, 3092–3096.

TAYLOR, G. I. (1952). The action of waving cylindrical tails in propelling microscopic organisms. *Proc. R. Soc.* **211**, 225–239.

YAMADA, H. (1970). *Strength of biological Materials*. Baltimore: Williams & Wilkins Comp.